ELSEVIER

Contents lists available at ScienceDirect

Sensors and Actuators: B. Chemical

journal homepage: www.elsevier.com/locate/snb





Spectrally filtered photodiode pairs for on-chip ratiometric aptasensing of cytokine dynamics

Zheshun Xiong ^{a,1}, Kewei Ren ^{b,1}, Matthew Donnelly ^a, Mingxu You ^{b,*}, Guangyu Xu ^{a,*}

- ^a Department of Electrical and Computer Engineering, University of Massachusetts, Amherst, MA 01003, USA
- ^b Department of Chemistry, University of Massachusetts, Amherst, MA 01003, USA

ARTICLE INFO

Keywords:
Ratiometric aptasensing
Cytokine dynamics
Spectrally filtered photodiode pairs
On-chip fluorescence sensing
Immune response monitoring

ABSTRACT

Miniaturized, cost-effective cytokine sensing devices are essential for health monitoring and critical care of patients with acute immune responses. Here we report an on-chip ratiometric aptasensing device to monitor the dynamics of an essential immune response biomarker, interferon-gamma. Our device is formed by pairs of spectrally filtered silicon photodiodes that are surface functionalized with aptamer probes. These photodiode pairs are able to rapidly detect two-color fluorescence changes transduced from aptamer-cytokine binding events within *c.a.* 6 min at picomolar levels, which are sufficient to capture the cytokine transients in point-of-care settings. Furthermore, our device can be reset to baseline by simple washing steps, yielding consistent readout in consecutive runs. Combined with their chip-scale construct and real-time operation, our cytokine sensors may have possible use in point-of-care and therapeutic screening applications.

1. Introduction

Immune response monitoring is essential in point-of-care (POC) applications such as the critical care of patients with acute immune responses [1,2]. Many human immune responses are associated with cytokine release syndrome, which needs to be rapidly identified by biosensors that can offer robust readout [3–6]. For instance, cytokine monitoring is significant to COVID-19 patients because excessive release of inflammatory cytokines in blood [7–9] such as interleukin 6 (IL-6), interferon-gamma (IFN- γ), and C-reactive protein (CRP) can be a fatal immune response if not identified in a timely manner, and needs to be closely monitored during the clinical treatment or vaccine development [10].

To offer an ultimate POC solution to understaffed conditions, an ideal cytokine biosensor should: 1) be miniaturized for integration purposes [11]; 2) record cytokine dynamics in a timely manner; and 3) feature crucial attributes such as low limit-of-detection, low drift, and high specificity [12]. Yet, these requirements have not been simultaneously met in today's sensing technologies. For instance, most electrochemical cytokine sensors suffer from signal drifting and device-to-device variation, and often require costly research-grade potentiostats [13–15]. On the other hand, most optical cytokine

sensors are noted for their robust operation, however limited by a bulky optical readout that can constrain their POC use [16–19]. To overcome these limitations, the ratiometric aptasensing strategy, in which aptamer-cytokine binding events are quantified by the fluorescence ratio of donors and acceptors in a Förster resonance energy transfer (FRET) pair, has been recognized for its reduced baseline drift and device-to-device variations [20–22]. If such sensing strategy can be achieved in devices with compact optical readout, we will be able to monitor cytokine dynamics in a miniaturized POC testing system, which will in the long term make an impact for personalized medicine.

To enable miniaturized ratiometric aptasensing, one pair of photodetectors should be placed next to each other, ideally built in a chip scale, and integrated with distinct on-chip spectral filters to detect the emission light of select donors and acceptors. To achieve this, the two on-chip filters need to be site-selectively patterned onto each of the two photodetectors. To assure high wavelength selectivity of the device, the transmittance spectra of these two filters need to feature: 1) low optical crosstalk to each other; 2) high rejection of the targeted excitation light; and 3) high transmittance of the targeted emission light. To date, such on-chip ratiometric aptasensors are still lacking, possibly challenged by the absence of methodology in patterning paired spectral filters specifically designed for ratiometric sensing.

E-mail addresses: mingxuyou@chem.umass.edu (M. You), guangyux@umass.edu (G. Xu).

^{*} Corresponding authors.

¹ These authors contributed equally to this work.

To this end, here we report an on-chip ratiometric aptasensing device to monitor the dynamics of an essential immune response biomarker, IFN- γ [23–25]. Our device is formed by pairs of spectrally filtered silicon photodiodes (*i.e.*, Si PD) that are surface functionalized with aptamer probes [26,27]. These PD pairs are able to rapidly detect two-color fluorescence changes transduced from aptamer-cytokine binding events within *c.a.* 6 min at picomolar (pM) levels, which are sufficient to capture the cytokine transients in POC settings [28–40]. Importantly, we demonstrate that our PD pairs can be reset to the original baseline by simple washing steps, yielding consistent readout in consecutive runs. Combined with its chip-scale construct and real-time operation, our device may be ultimately integrated in bedside blood testing systems for a variety of health monitoring and therapeutic screening uses.

2. Material and methods

2.1. Array fabrication

We first patterned Cr on a Si/SiO $_2$ substrate to serve as a contact for n-doped α -Si. Next, n-doped (n, 40 nm), un-doped (i, 600 nm), and p-doped (p, 40 nm) α -Si layers were sequentially deposited by 200 °C plasma-enhanced chemical vapor deposition (PECVD) steps. After that, the p-i-n layers were patterned by reactive-ion etching (RIE) into 2-by-3 120 μ m \times 300 μ m sized photodiode (PD) pixels, and passivated by a 30 nm Al $_2$ O $_3$ film based on atomic layer deposition at 250 °C. We then applied buffered oxide etching to create contact openings, followed by sputtering of \sim 120 nm indium tin oxide (ITO) to contact p-doped α -Si. Next, Cr/Au layers (10/200 nm) were deposited on the pad area, followed by passivating the array with a 4 μ m-thick SU-8 layer (Fig. S1).

After the SU-8 passivation step, we sequentially patterned two distinct photoresist-based spectral filters onto select columns of the 2by-3 array, yielding 3 pairs of PD pixels (i.e. PD pairs) for selective detection of the emission signals of Alexa Fluor 555 (AF555) and Cy5, which were chosen as donors and acceptors of the FRET pair, respectively. Specifically, the AF555 [Cy5] spectral filter was made by mixing visible light absorbing dyes (Epolin), Epolight 5391 (3.5 wt%), Epolight 5262 (0.25 wt%), and Epolight 6661 (3.5 wt%) [Epolight 5391 (3.5 wt %) and Epolight 5822 (2.0 wt%)] into NR9-1000PY (Futurrex) photoresist. Subsequently, the AF555 filter (\sim 2.8 μm thick) was first spun onto the array (800 rpm, 40 s) and thermally crosslinked (150 °C, 2 h) to reduce the solubility of the layer in subsequent photoresist coatings. Next, a KL6008 photoresist layer was patterned to act as a hard mask for dry etching. The AF555 filter was then patterned by reactive-ion etching over one column of the array and passivated by another 4 μ m-thick SU-8 layer. The same process was then repeated for the Cy5 filter on the other column of the array. The spectrally filtered PD array was then wirebonded to a printed circuit board (PCB) and packaged with a polydimethylsiloxane (PDMS) based microfluidic channel via O2-plasma assisted binding. Metallic and plastic tubing were inserted into the inlet and outlet of the microfluidic channel for introducing analytes to the

2.2. Device characterization

To characterize the optical properties of the spectral filters, we spin coated them onto 100 μ m-thick glass coverslips (Fisher Scientific) and measured their transmission spectra by an UV–vis-NIR spectrometer (SHIMADZU 3600).

The *I-V* measurements of PD pairs were measured by Keysight B1500A with 100 mV sweep step of the voltage bias across each pixel, V_{bias} ; pixels were illuminated at 550/15 nm (260 mW at 100 %), 575/25 nm (310 mW at 100 %), or 640/30 nm (231 mW at 100 %)

wavelengths, provided by FN1 through a CFI6O Plan Achromat $10\times$ objective lens (NA = 0.25, Nikon). At the array level, we built an offboard multiplexing circuit in a home-made faradic cage, using two ADG406 multiplexers and two CD4029BMS counters to select pixels and bias them at $V_{\rm bias} = -5$ V with Keysight B2902A. The pixel current was amplified to a voltage readout, $V_{\rm out}$, by a low-noise preamplifier SR570 (Stanford Research Systems), followed by a Hum bug noise eliminator (A-M Systems) to remove 50/60 Hz noise. The preamplifier operated in the low noise mode, with 5 uA/V sensitivity, and a 100 Hz cutoff frequency of a low-pass signal filter (12 dB/octave to reduce the high-frequency noise in the recorded $V_{\rm out}$ trace), all of which were optimized to maximize the signal-to-background and signal-to-noise ratios (i.e. SBR and SNR) obtained from the $V_{\rm sig}$ data. The resulting $V_{\rm out}$ -trace and the clock signal were recorded by an 8-channel with 256 MS buffer memory digital oscilloscope (Pico 4824).

2.3. DNA functionalization

Analytes used in our experiment are as follows: 1 mg ml^{-1} biotinylated bovine serum albumin (BSA) in ultrapure water (Thermofisher); 0.2 mg ml^{-1} AF555 conjugated streptavidin in $1 \times \text{phosphate}$ buffered saline (PBS, Thermofisher); $1 \mu \text{M}$ biotinylated Cy5-labeled IFN- DNA aptamers in ultrapure water. Here $1 \times \text{PBS}$ is the standard PBS solution with 137 mM NaCl. The biotinylated BSA, native streptavidin, and AF555 conjugated streptavidin, and native streptavidin were purchased from Sigma Aldrich; the recombinant human IFN- γ was purchased from R&D systems; DNA aptamers were purchased from Integrated DNA Technologies, whose 3' and 5' ends were biotinylated and labeled with Cy5, respectively. The aptamer sequence is 3'-biotin-CCCCAACCTGTGTTGTGGGGTTGTGTTGGTTGGGG-Cy5-5'.

The aforementioned analytes were sequentially injected to the microfluidic channel by a pipettor with 200 μL tips at room temperature, followed by a washing step (9 mL deionized (DI) water injected by a 5 mL syringe) at room temperature to remove extra analytes. In particular, 80 μL biotinylated BSA were introduced to the surface of the SU-8 passivated PD pairs for 1 h, allowing them to be physically adsorbed to the SU-8 surface. Next, 80 μL AF555 conjugated streptavidin were introduced for 10 min in the dark. Finally, 80 μL biotinylated Cy5-labeled IFN- γ DNA aptamers were introduced and immobilized for 2 h in the dark. Prior to the biosensing experiments, the PD array was kept in DI water and stored in the dark at room temperature.

2.4. Biosensing experiments

During the 1st run of control [IFN-y aptasensing] experiment, we first immersed the array in $1 \times PBS$, then sequentially introduced 0.1 pM -1 nM native streptavidin (i.e., not conjugated with AF555) [IFN-γ] mixed in 80 μ L 1 \times PBS at 15-min intervals. At the end of the 1 nM interval, we washed the array with 15 mL DI water pre-warmed at c.a. 55 °C for 6 min to dissociate the IFN- γ from the aptamers and reset the array (note: this washing temperature was experimentally tested, see Fig. S2), followed by a 24-min interval before the 2nd run. We then re-introduced the same 1 \times PBS, 0.1 pM - 1 nM analytes, and 55 $^{\circ}$ C DI washing steps to the array in the 2nd run. Afterwards, we re-immersed the array with $1 \times PBS$ again at room temperature to reset V_{sig} values. The 550/15 nm excitation light (with 260 mW at 100 %) was applied using an epifluorescence upright microscope (FN1, Nikon) equipped with a SPECTRA X light engine (Lumencor). NIS-Elements Advanced Research software (Nikon) was used to automate the microscope and provide the clock signal (Fig. S3).

Statistical analysis was based on Student's t-test (two-tailed, independent two-sample t-test).

3. Results and discussion

3.1. Experimental setup

We designed our ratiometric aptasensing assay by first choosing AF555 and Cy5 as donors and acceptors of the FRET pair for their high brightness, photostability, and FRET efficiency. We estimated the AF555-Cv5 FRET efficiency to change from 1 before IFN-y binding to 0.0163-0.0303 after IFN-y binding based on the quantum yield, orientation factors, and spectral overlap of the donor/acceptor pair (Fig. S4). To enable on-chip ratiometric aptasensing, we chose to functionalize the spectrally-filtered PD pairs (see details below) by sequentially adding biotinylated BSA, AF555-conjugated streptavidin, and biotinylated Cy5-labeled DNA aptamer probe designed to specifically bind to IFN-γ [33,35,36,38,41], which link together via the strong biotin-streptavidin binding [42-44]. This aptamer probe will self-hybridize itself to form a hairpin structure when no IFN-y binds to it, pulling Cy5 close to AF555 to form a FRET pair with AF555 [Cy5] being the donor [acceptor]. When IFN-y binds to the aptamer probe, the hairpin structure of the aptamer will open up and separate Cv5 and AF555 apart. Such structure change in the aptamer will then lessen the FRET effect, leading to an increase [decrease] of the AF555 [Cv5] emission signals under 550/15 nm excitation (Fig. 1a).

On the device side, we fabricated Si PD pairs in a 2-by-3 cross-bar array as we reported before [45,46]. Briefly, these Si PDs were patterned from PECVD based α-Si layers (p-i-n structured, chosen for their improved sensitivity over p-n diodes [47]), contacted by ITO and Cr layers at their p- and n-terminals, and passivated by a SU-8 layer which was tested to be chemically stable after crosslinking and is optically transparent to the wavelengths used in this work [48,49]. We then developed two spectral filters targeting AF555 emission and Cy5 emission signals by mixing the light absorbing dyes into optically transparent photoresist, respectively [46]. Specifically, the AF555 [Cy5] filter was optimized to 1) block the AF555 excitation light (provided by an upright fluorescence microscope) peaked at 555 nm, 2) block the Cy5 [AF555] emission light peaked at 666 nm [580 nm], and 3) pass the AF555 [Cy5] emission light peaked at 580 nm [666 nm] (Fig. 1b). As a result, both filters featured > 10² extinction ratios, with their transmittance at targeted [blocked] wavelengths being > 10 % [< 0.1 %]. Afterwards, we sequentially patterned these two filters onto select columns in the 2-by-3 array, yielding 3 pairs of PD pixels that could selectively detect AF555 and Cy5 signals (named as AF555 and Cy5 pixels here), respectively (Fig. 1c). In particular, we thermally crosslinked the first filter (AF555) spun on the PD pairs, patterned it *via* a dry etching step, passivated it with a SU-8 layer, and repeated the same procedure for the second filter. (Cy5, see Section 2.1). With the device dimension we chose, optical crosstalk among our PD pixels should be largely decided by the extinction ratios of the two filters.

The spectrally-filtered PD array was then wire-bonded onto a PCB, characterized by its responses under select wavelengths (see below), and packaged in a PDMS based microfluidic channel (Fig. 1d). Using this microfluidic channel, we were able to sequentially inject aforementioned BSA, streptavidin, and DNA aptamer probes (with a pipettor) through the inlet, which served to functionalize the spectrally filtered PDs for aptasensing experiments under an upright fluorescence microscope.

3.2. Wavelength selectivity and pixel-to-pixel variation

To examine the wavelength selectivity and the pixel-to-pixel variation of the PD array [46], we first collected the I-V curves of all 6 spectrally filtered pixels (3 AF555 and 3 Cy5 pixels) before packaging them into the PDMS channel (Fig. 2). We biased each pixel with $V_{\rm bias}$ ranging from +3 V to -5 V and illuminated at 550/15 nm (with 260 mW at 100 %), 575/25 nm (with 310 mW at 100 %), and 640/30 nm (with 231 mW at 100 %) wavelengths, with the light power (I_{light}) ranging from 10 % to 100 % (Fig. 2a, b). These three wavelengths were chosen to characterize the wavelength selectivity as they fall into the excitation spectra and the emission spectra of AF555 and the emission spectra of Cy5, respectively (Fig. 1b). We observed that all 6 pixels showed: 1) a rectified I-V as we expected in p-i-n structured PDs, and 2) a forward turn-on voltage of around 1–1.5 V, likely due to the high doping levels in the α -Si layers or the series resistance of the ITO contact lines [45]. To quantify the effect of the light power (I_{light}), the wavelength, and the pixel bias (V_{bias}), we define the photocurrent (I_{ph}) as the light-on current subtracted by the dark current measured from each PD pixel (Fig. 2c). As expected, our results show that $I_{\rm ph}$ at all 3 wavelengths increases with I_{light} and the V_{bias} amplitude. Notably, we observed that:

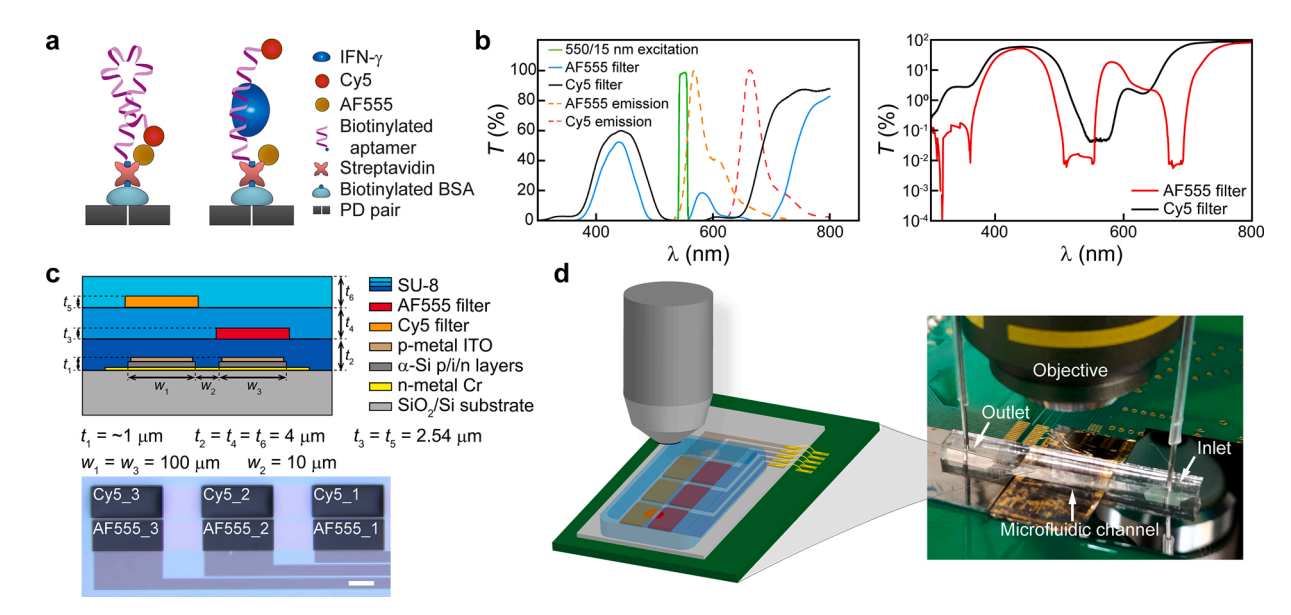


Fig. 1. Experimental setup. (a) Illustration of on-chip ratiometric aptasensing of IFN-γ with a PD pair. (b) Filter design, including the 550/15 nm excitation filter, the emission spectra of AF555 and Cy5, and the transmission spectra of AF555 and Cy5 filters in a linear scale (left) and a logarithmic scale (right). (c) Illustration of a spectrally-filtered PD array composed of 3 pairs of AF555 and Cy5 pixels. Scale bar, 100 μm. (d) Illustration (left) and image (right) of the experimental setup. The PD array is packaged in a microfluidic channel (with an inlet and an outlet), wire bonded onto a PCB, and aligned to the objective of an upright fluorescence microscope.

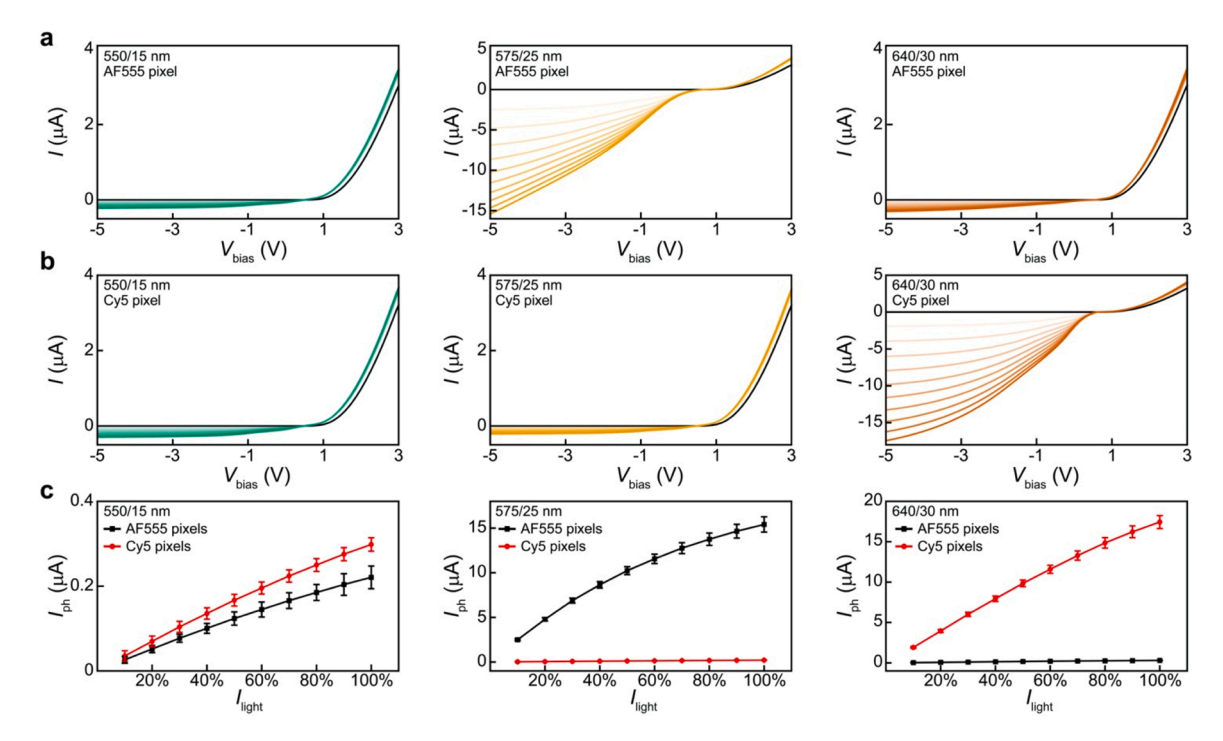


Fig. 2. Wavelength selectivity and pixel-to-pixel variation. (a) Measured I-V_{bias} curves of an AF555 pixel at 550/15 nm (left) with I_{light} ranging from 26 mW (10 %) to 260 mW (100 %), 575/25 nm (middle) with I_{light} ranging from 31 mW (10 %) to 310 mW (100 %), and 640/30 nm (right) with I_{light} ranging from 23.1 mW (10 %) to 231 mW (100 %). (b) Measured I-V_{bias} curves of a Cy5 pixel at 550/15 nm (left), 575/25 nm (middle), and 640/30 nm (right) wavelengths. (c) I_{ph} vs I_{light} with the pixels biased at V_{bias} = -5 V and illuminated at 550/15 nm (left), 575/25 nm (middle), and 640/30 nm (right) wavelengths. Statistics are based on measurements from 3 AF555/Cy5 pixels. The error bars represent ± 1 s.d.

1) the extinction ratios of the AF555 pixel ($I_{575\mathrm{nm},100}$ %/ $I_{550\mathrm{nm},100}$ % and $I_{575\mathrm{nm},100}$ %/ $I_{640\mathrm{nm},100}$ % at $V_{\mathrm{bias}}=-5$ V) and the Cy5 pixel ($I_{640\mathrm{nm},100}$ %/ $I_{550\mathrm{nm},100}$ % and $I_{640\mathrm{nm},100}$ %/ $I_{575\mathrm{nm},100}$ % at $V_{\mathrm{bias}}=-5$ V) were (69.8 \pm 3.9, 50.1 \pm 2.8) and (58.5 \pm 2.7, 82.3 \pm 3.8), respectively, suggesting good wavelength selectivity of the spectrally filtered PD pairs; 2) the pixel-to-pixel variation at $V_{\mathrm{bias}}=-5$ V among the 3 AF555 [Cy5] pixels is less than 6 % [5 %] when I_{light} at 575/15 nm [640/30 nm] is 310 mW [231 mW], suggesting good uniformity across the array in detecting the AF555 [Cy5] signal.

To conduct real-time ratiometric aptasensing, we need to constantly switch between AF555 and Cy5 pixels and trace their $I_{\rm ph}$ values before packaging them into the PDMS channel (Fig. 3). To achieve this, we built an off-board multiplexing circuit to alternately bias the select AF555 and Cy5 pixels at $V_{\rm bias}=-5$ V as we reported before [46], where a clock signal ($t_{\rm on}/t_{\rm off}=10/20$ ms) synchronized with the microscope was employed to trigger the pixel switching. Specifically, the pixel current was pre-amplified into a voltage readout ($V_{\rm out}$), filtered by a 100 Hz low-pass filter, and passed through a 50/60 Hz noise eliminator. Using this setup, we sequentially record a 3-s $V_{\rm out}$ -trace from each pixel (0.2 ms per sample) using a digital oscilloscope with a 256 MS buffer memory (Fig. 3a, measured in the dark), where $V_{\rm out}$ values were found to reach to the steady state within 0.1 s.

To evaluate the readout of our PD pairs to weak AF555/Cy5 emission signals in this setup, we characterized AF555 and Cy5 pixels under $64\times$ attenuated $I_{\rm light}$ at 575/25 nm and 640/30 nm, respectively, by applying neutral density filters in the optical path of the microscope. Consequently, we observed that the $V_{\rm out}$ values of AF555 [Cy5] pixels under $64\times$ attenuated 575/25 nm [640/30 nm] illumination (showcased with $I_{\rm ph}$ being 100 % in Fig. 3b) were well separated from those measured in the dark, and well beyond their noise floor in the $V_{\rm out}$ -trace, suggesting good SBR and SNR values, respectively. On the other hand, the $V_{\rm out}$ values of AF555 [Cy5] pixels under $64\times$ attenuated 575/25 nm [640/30 nm] illumination were on par with those under non-attenuated 550/15 nm and 640/30 nm [575/25 nm] illumination, which reaffirmed the

wavelength selectivity of our spectrally filtered array in this V_{out} -tracing setup (Fig. 3b).

3.3. Linearity and limit of detection

We next quantified PD responses at various I_{light} values to evaluate the light-detection limit of the array. To achieve this, we chose to average the recorded Vout values (subtracted by those measured in the dark, i.e., no light was illuminating the array) from 0.1 s to 3 s as the pixel signal, V_{sig} , during each scan of the 2-by-3 array. Accordingly, we obtained V_{sig} values from each pixel under 550/15 nm, 575/25 nm, and 640/30 nm illumination with I_{light} ranging from 10 % to 100 % (note: an additional 64× attenuation was applied to the 575/25 nm and 640/ 30 nm illumination on AF555 and Cy5 pixels, respectively). Our results showed good linearity in $V_{\text{sig}}-I_{\text{light}}$ relationships ($R^2>0.97,$ Fig. 3c) and high SBR values (SBR > 3 as we defined previously [46], Fig. 3d) in both AF555 and Cy5 pixels at all 3 wavelengths, suggesting that our PD pairs can linearly respond to AF555/Cy5 emission signals with statistically significant V_{sig} data. Furthermore, SBR values of AF555 [Cy5] pixels at 575/25 nm [640/30 nm] illumination were larger than 6 for I_{light} down to 0.48 mW [0.36 mW] (i.e. 10 % plus 64× attenuation), suggesting the low light-detection limit of the array. Last but not the least, AF555 [Cy5] pixels showed comparable SBR values under 64× attenuated 575/25 nm [640/30 nm] illumination to those under non-attenuated 550/15 nm and 640/30 nm [575/25 nm] illumination, which echoes to the wavelength selectivity shown in Fig. 2c and b.

3.4. Biosensing experiment

After the array characterization steps, we packaged the PD array into a microfluidic channel \emph{via} O₂-plasma assisted PDMS binding, where metallic and plastic tubing were inserted into the inlet and outlet for injection and removal of analytes (Fig. 1d). We then functionalized the PD array with BSA, streptavidin, and DNA aptamers (see Section 2.3),

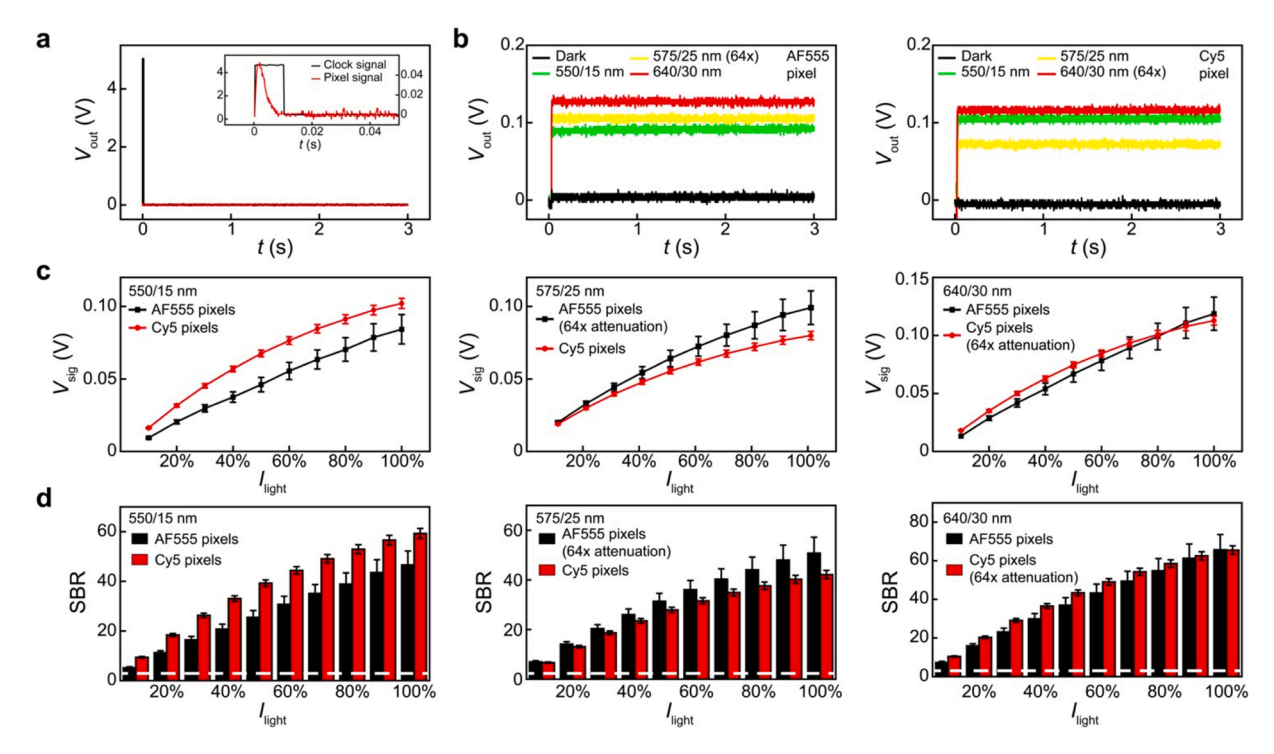


Fig. 3. Linearity and limit of detection. (a) Measured 3 s V_{out} -trace of one pixel in the dark (0.2 ms per sample) and the clock signal employed for array scanning. The pixel signal ($V_{\rm sig}$) is averaged from the 0.1 to 3 s data in the $V_{\rm out}$ -trace. (b) Measured 3 s V_{out} -traces of an AF555 (left) and a Cy5 (right) pixel when the array is in the dark or illuminated at 550/15 nm, 575/25 nm (64× attenuation for the AF555 pixel), and 640/30 nm (64× attenuation for the Cy5 pixel) wavelengths, all with $I_{\rm light}$ being 100 %. (c) $V_{\rm sig}$ vs $I_{\rm light}$ under 550/15 nm (left), 575/25 nm (middle, 64× attenuation for AF555 pixels), and 640/30 nm (right, 64× attenuation for Cy5 pixels) illuminations. (d) Measured SBR values under 550/15 nm (left), 575/25 nm (middle, 64× attenuation for AF555 pixels), and 640/30 nm (right, 64× attenuation for Cy5 pixels) illuminations. Dashed lines indicate SBR = 3. In (c) and (d), statistics are based on measurements from 3 AF555/Cy5 pixels. The error bars represent ± 1 s.d.

followed by removing unbound proteins/aptamers by a 9 mL DI water washing step at room temperature. The functionalized PD array was then sequentially applied for control and IFN- γ aptasensing experiments. In both experiments (Fig. 4), we first immersed the array in $1 \times PBS$, then sequentially introduced 0.1 pM-1 nM native streptavidin or IFN-7 mixed in $1 \times PBS$ at 15-min intervals. At the end of the 1 nM interval, we washed the array with DI water pre-warmed at c.a. 55 °C to dissociate the IFN-y bound to aptamers and reset the array (the 6-min gray zones when transient data were not shown), followed by a 24-min interval to cool down the array back to room temperature and stabilize its readout. We then repeated the same $1 \times PBS$, 0.1 pM – 1 nM analytes, and 55 °C DI washing steps again as the 2nd run of the array. Such two consecutive runs of the array served to examine the robustness and reusability of PD pairs in both control and aptasensing experiments. Throughout the experiments, we used an upright fluorescence microscope to illuminate the PD array with 260 mW 550/15 nm excitation light pulsed at t_{on} / $t_{\rm off} = 18/162$ s (i.e., in a 3-min period) to alleviate the photobleaching effect.

In two consecutive runs of the control experiment, we introduced native streptavidin to the array, and observed $< 5 \% V_{\rm sig}$ change in *both* AF555 *and* Cy5 pixel signals as we expected (Fig. 4a, b), since native streptavidin does not bind to the DNA aptamer. In contrast, we introduced IFN- γ to the array in two consecutive runs of the aptasensing experiment, and observed that $V_{\rm sig}$ values of all 3 AF555 [Cy5] pixels increased [decreased] as the IFN- γ concentration increased from 0.1 pM to 10 pM (Fig. 4a, b), which settled to the steady state at each concentration within 6 min (*i.e.*, at the 2nd reading) [38]. This PD response can be attributed to the structural change of DNA aptamers due to aptamer-IFN- γ binding events, which separated the AF555 and Cy5 dyes apart and lessened the FRET effect. Due to this structural change, less AF555 emission light is allocated to excite Cy5, leading to an increase [a decrease] in AF555 [Cy5] emission signals as detected by their

corresponding pixels. On the other side, the V_{sig} values in both AF555 and Cy5 pixel did not further increase when 100~pM-1~nM IFN- γ was introduced, likely because the DNA aptamers on PD pixels had been saturated by the end of 10~pM IFN- γ interval.

We then quantified the ratiometric readout of the PD pairs at each concentration, which is defined as the ratio of $V_{\text{sig_AF555}}/V_{\text{sig_Cy5}}$ normalized by the value when PDs were immersed in $1 \times PBS$ before the 1st run of the control/aptasensing experiment (Fig. 4c, d) [50,51]. The results show that our PD pairs indeed ratiometrically detected IFN-y dynamics with the limit-of-detection (LOD) being as low as 1 pM, when the PD readout is significant compared to those in the control experiment. We repeated this analysis in another independent experiment with another PD array, which also showed 1 pM LOD (Fig. S5). Such pM-level detection of IFN-y dynamics, together with its fast response (c.a. 6-min settling time at each IFN-γ concentration), hold promise to capture the cytokine transients in POC applications such as the critical care of patients with acute immune responses [3,25]. It is encouraging to note that at all concentrations the ratiometric readout has < 1 % relative standard deviation (RSD) in each PD pair, and < 4 % RSD across all 3 pairs (obtained from 2nd to 5th readings in Fig. 4c). These results suggested that our PD pairs indeed featured low drift and low pair-to-pair variation due to the ratiometric aptasensing mechanism.

Importantly, we found that our PD pairs can also be reset to the original baseline by the 55 °C DI washing steps, yielding consistent readout in two consecutive runs. In particular, followed by the 1st 55 °C DI washing step, we re-immersed the PD pairs in 1 × PBS, and observed that $V_{\rm sig}$ values across the array returned to their baseline values (i.e., $V_{\rm sig,baseline}$ when PDs were immersed in 1 × PBS before applying 0.1 pM streptavidin/IFN- γ for the 1st time) with < 2 % in difference (Fig. 4a–c). This result suggested that the 55 °C DI washing effectively dissociated IFN- γ from the aptamers, while keeping AF555-conjugated streptavidin and Cy5-labeled aptamers on the array. Consequently, the following 2nd

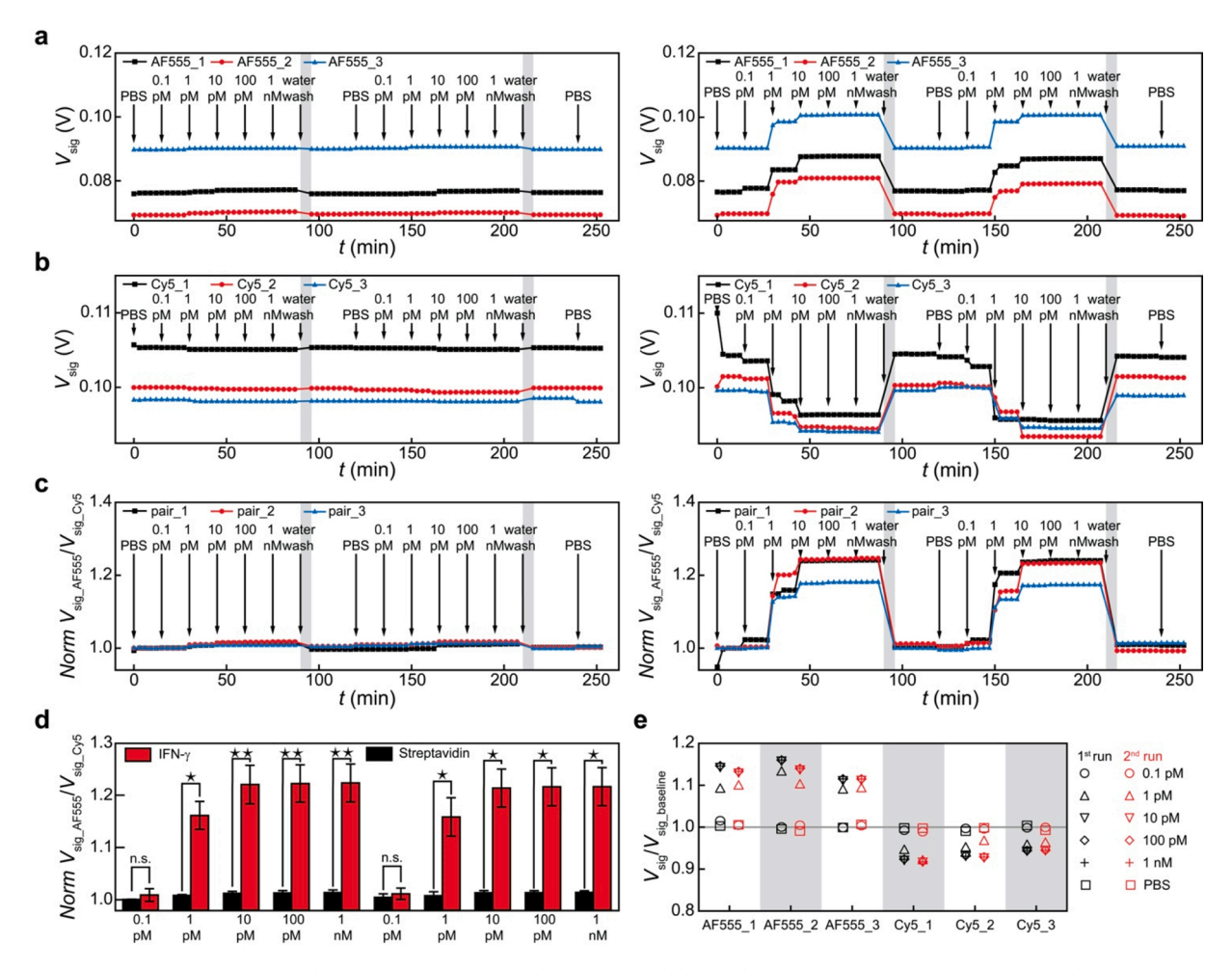


Fig. 4. Biosensing experiments. (a) Measured V_{sig} -traces of 3 AF555 pixels in the control (left) and IFN-γ aptasensing (right) experiments. (b) Measured V_{sig} -traces of 3 Cy5 pixels in the control (left) and IFN-γ aptasensing (right) experiments. (c) Ratiometric readout of 3 PD pairs in the control (left) and IFN-γ aptasensing (right) experiments. (d) Ratiometric readout v_s . analyte concentration in the control (black) and IFN-γ aptasensing (red) experiments. Statistics are based on measurements from 3 PD pairs; the errors bars represent ±1 s.d.; n.s. p > 0.05, *p < 0.05, *p < 0.05, *p < 0.05 based on Student's t-test. (e) $V_{\text{sig}}/V_{\text{sig_baseline}}$ of all 6 PD pixels in two consecutive runs of the IFN-γ aptasensing experiments. In (a)–(c), arrows pointed to the moment when the corresponding analyte was introduced to the array; grey windows represent the 6-min periods of 55 °C DI washing steps (For interpretation of the references to colour in this figure legend, the reader is referred to the web version of this article).

run of control/aptasensing experiments yielded similar 0.1~pM - 10~nM $V_{\rm sig}$ values to those obtained in the 1st run. And the 2nd 55 °C DI washing step afterwards can reset $V_{\rm sig}$ values (with PDs immersed in $1 \times PBS$) back to their $V_{\text{sig_baseline}}$ values once again. Quantitatively, V_{sig} values from two runs of aptasensing experiments (normalized by V_{sig} $_{\text{baseline}}$ values) at each IFN- γ concentration have < 3 % in difference (Fig. 4e). Such repeatable readout of our PD pairs is likely due to the high dissociation constant of the aptamer we chose ($K_D = 3.4 \text{ nM}$ specific to IFN-γ, [31]) as well as the low-ion environment (DI water) we used for washing [52]. The resulting mild aptamer-IFN-γ binding can thus be dissociated by warm DI water, resetting the PD readout for the following aptasensing experiment [34-37]. These results suggest that comparing with other types of cytokine receptors (e.g., antibodies), our aptamer probes feature: 1) high thermal stability that allows them to go through 55 °C DI washing steps without being degraded [53,54], and 2) design flexibility on the aptamer sequences to fine tune their dissociation constant specific to the targeted cytokines [53-55].

We remark that the LOD of our ratiometric aptasensing array is on par with most prior electrochemical and optical IFN- γ aptasensors (Table 1). Compared to prior IFN- γ detection works [28–40], our device demonstrated a practically useful LOD and robust reusability with no complex surface chemistry steps. On the other hand, the signal drift of all 3 PD pairs at all IFN- γ concentrations is on par with prior optical

IFN- γ aptasensors, and more than 37.5 % lower than prior electrochemical IFN- γ aptasensors [38]. Last but not least, the dynamic range of our device is likely limited by the number of aptamers immobilized on the PD pairs, which may be improved by increasing the PD areas and/or switching to other surface functionalization strategies with higher immobilization densities [37,56,57]. If successful, such miniaturized device platform may provide a viable alternative approach to build next-generation POC testing systems.

4. Conclusion

In sum, we report an on-chip ratiometric aptasensing device to monitor the dynamics of IFN- γ with low LOD, fast settling time, low signal drift, low variation, and robust reusability. Our device is formed by spectrally filtered Si PD pairs that are functionalized with DNA aptamer probes, which can rapidly detect two-color fluorescence changes transduced from aptamer-cytokine binding events within *c.a.* 6 min down to pM levels. Such LOD is on par with most prior electrochemical and optical cytokine sensors, and is sufficient to capture cytokine transients in practical POC settings. Importantly, we demonstrate that our PD pairs can be reset to the original baseline by simple washing steps, yielding consistent readout in consecutive runs. Combined with its chip-scale construct and real-time operation, our device

Table 1 Comparison of IFN- γ detection works.

Detection method	LOD (pM)	Real-time operation	Reusability	Settling time	Drift	Reference
Graphene-FET	83	Not shown	Not shown	Not shown	Not shown	[28]
Spectroscopy	5.9	Not shown	Not shown	Not shown	Not shown	[29]
Spectroscopy	1.75×10^{-4}	Shown	Not shown	30 min	< 1 % in 90 min	[30]
Spectroscopy	5×10^3	Shown	Not shown	15 min	Not available	[31]
SPR ^a	33	Shown	Shown	20 min	Not available	[32]
Microscopy	1	Not shown	Not shown	Not shown	Not shown	[33]
ARROW ^b	29.4	Shown	Shown	60 s	~ 3 % in 40 s	[34]
SWV^c	0.35	Shown	Shown	c.a. 1-8 min	~14.6 % in 5 min	[35]
SWV	1.1	Not shown	Shown	Not shown	Not shown	[36]
SWV	60	Not shown	Shown	15 min	Not shown	[37]
SWV	10^{-4}	Shown	Shown	5 min	~1.6 % in 4 min	[38]
CV^d	100	Not shown	Not shown	Not shown	Not shown	[39]
DPV ^e	2	Not shown	Not shown	> 1 h	Not shown	[40]
PD pairs	1	Shown	Shown	6 min	<1 % in 12 min $$	This work

^a Surface plasmon resonance.

may provide a robust platform that can ultimately be integrated in bedside blood testing systems for health monitoring and therapeutic screening uses.

CRediT authorship contribution statement

Zheshun Xiong: Methodology, Investigation, Writing - original draft. Kewei Ren: Methodology, Writing - review & editing. Matthew Donnelly: Methodology, Investigation, Writing - original draft. Mingxu You: Methodology, Funding acquisition, Writing - review & editing. Guangyu Xu: Conceptualization, Supervision, Methodology, Funding acquisition, Writing - original draft, Writing - review & editing.

Declaration of Competing Interest

The authors report no declarations of interest.

Acknowledgements

This work was supported by the National Science Foundation under ECCS-1835268, ECCS-2046031, and CBET-1846152.

Appendix A. Supplementary data

Supplementary material related to this article can be found, in the online version, at doi:https://doi.org/10.1016/j.snb.2021.130330.

References

- R. Snyderman, Personalized health care: from theory to practice, Biotechnol. J. 7 (2012) 973–979.
- [2] M. Salem, B. Chernow, R. Burke, J. Stacey, M. Slogoff, S. Sood, Bedside diagnostic blood testing: its accuracy, rapidity, and utility in blood conservation, JAMA 266 (1991) 382–389.
- [3] J.M. Cliff, S.H.E. Kaufmann, H. McShane, P. Helden, A. O'Garra, The human immune response to tuberculosis and its treatment: a view from the blood, Immunol. Rev. 264 (2015) 88–102.
- [4] A. Shimabukuro-Vornhagen, P. Gödel, M. Subklewe, H.J. Stemmler, H.A. Schlößer, M. Schlaak, M. Kochanek, B. Böll, M.S. von Bergwelt-Baildon, Cytokine release syndrome, J. Immunother. Cancer 6 (2018) 1–14.
- [5] D.W. Lee, R. Gardner, D.L. Porter, C.U. Louis, N. Ahmed, M. Jensen, S.A. Grupp, C. L. Mackall, Current concepts in the diagnosis and management of cytokine release syndrome, Blood 124 (2014) 188–195.
- [6] H.H. Yiu, A.L. Graham, R.F. Stengel, Dynamics of a cytokine storm, PLoS One 7 (2012), e45027.
- [7] J.B. Moore, C.H. June, Cytokine release syndrome in severe COVID-19, Science 368 (2020) 473–474.
- [8] T. Hirano, M. Murakami, COVID-19: a new virus, but a familiar receptor and cytokine release syndrome, Immunity 52 (2020) 731–733.

- [9] X. Sun, T. Wang, D. Cai, Z. Hu, H. Liao, L. Zhi, H. Wei, Z. Zhang, Y. Qiu, J. Wang, A. Wang, Cytokine storm intervention in the early stages of COVID-19 pneumonia, Cytokine Growth Factor Rev. 53 (2020) 38–42.
- [10] G.S. Ginsburg, K.A. Phillips, Precision medicine: from science to value, Health Aff. 37 (2018) 694-701.
- [11] H. Craighead, Future lab-on-a-chip technologies for interrogating individual molecules, Nature 442 (2006) 387–393.
- [12] M.C. Frost, M.E. Meyerhoff, Real-time monitoring of critical care analytes in the bloodstream with chemical sensors: progress and challenges, Annu. Rev. Anal. Chem. 8 (2015) 171–192.
- [13] B.S. Ferguson, D.A. Hoggarth, D. Maliniak, K. Ploense, R.J. White, N. Woodward, K. Hsieh, A.J. Bonham, M. Eisenstein, T.E. Kippin, K.W. Plaxco, Real-time, aptamer-based tracking of circulating therapeutic agents in living animals, Sci. Transl. Med. 5 (2013), 213ra165.
- [14] N. Arroyo-Currás, P. Dauphin-Ducharme, G. Ortega, K.L. Ploense, T.E. Kippin, K. W. Plaxco, Subsecond-resolved molecular measurements in the living body using chronoamperometrically interrogated aptamer-based sensors, ACS Sens. 3 (2018) 360–366.
- [15] H. Li, N. Arroyo-Currás, D. Kang, F. Ricci, K.W. Plaxco, Dual-reporter drift correction to enhance the performance of electrochemical aptamer-based sensors in whole blood, J. Am. Chem. Soc. 138 (2016) 15809–15812.
- [16] H. Zhu, S.O. Isikman, O. Mudanyali, A. Greenbaum, A. Ozcan, Optical imaging techniques for point-of-care diagnostics, Lab Chip 13 (2013) 51–67.
- [17] M. Singh, J. Truong, W.B. Reeves, J.-I. Hahm, Emerging cytokine biosensors with optical detection modalities and nanomaterial-enabled signal enhancement, Sensors 17 (2017) 428.
- [18] A.M. Dennis, W.J. Rhee, D. Sotto, S.N. Dublin, G. Bao, Quantum dot-fluorescent protein FRET probes for sensing intracellular pH, ACS Nano 6 (2012) 2917–2924.
- [19] A. Shalabney, I. Abdulhalim, Sensitivity-enhancement methods for surface plasmon sensors, Laser Photon. Rev. 5 (2011) 571–606.
- [20] S. Zhang, V. Metelev, D. Tabatadze, P.C. Zamecnik, A. Bogdanov Jr., Fluorescence resonance energy transfer in near-infrared fluorescent oligonucleotide probes for detecting protein-DNA interactions, Proc. Natl. Acad. Sci. U. S. A. 105 (2008) 4156–4161.
- [21] J. Shi, F. Tian, J. Lyu, M. Yang, Nanoparticle based fluorescence resonance energy transfer (FRET) for biosensing applications, J. Mater. Chem. B Mater. Biol. Med. 3 (2015) 6989–7005.
- [22] F. Lin, B. Yin, J. Deng, X. Fan, Y. Yi, C. Liu, H. Li, Y. Zhang, S. Yao, Fluorescence resonance energy transfer aptasensor for platelet-derived growth factor detection based on upconversion nanoparticles in 30% blood serum, Anal. Methods 5 (2013) 699–704.
- [23] M. Pai, L.W. Riley, J.M. Colford Jr., Interferon-gamma assays in the immunodiagnosis of tuberculosis: a systematic review, Lancet Infect. Dis. 4 (2004) 761–776
- [24] J.A. Green, S.R. Cooperband, S. Kibrick, Immune specific induction of interferon production in cultures of human blood lymphocytes, Science 164 (1969) 1415–1417.
- [25] E.P. Moura, V.P.C.P. Toledo, M.H.P. Oliveira, S. Spíndola-de-Miranda, H. M. Andrade, T.M.P.D. Guimarães, Pulmonary tuberculosis: evaluation of interferon-gamma levels as an immunological healing marker based on the response to the Bacillus Calmette-Guerin, Mem. Inst. Oswaldo Cruz 99 (2004) 283-287
- [26] C. Cao, F. Zhang, E.M. Goldys, F. Gao, G. Liu, Advances in structure-switching aptasensing towards real time detection of cytokines, Trends Analyt. Chem. 102 (2018) 379–396.
- [27] Q. Zhu, G. Liu, M. Kai, DNA aptamers in the diagnosis and treatment of human diseases, Molecules 20 (2015) 20979–20997.

^b Antiresonant reflecting optical waveguide.

^c Square wave voltammetry.

^d Cyclic voltammetry.

^e Differential pulse voltammetry.

- [28] S. Farid, X. Meshik, M. Choi, S. Mukherjee, Y. Lan, D. Parikh, S. Poduri, U. Baterdene, C.E. Huang, Y.Y. Wang, P. Burke, Detection of Interferon gamma using graphene and aptamer based FET-like electrochemical biosensor, Biosens. Bioelectron. 71 (2015) 294–299.
- [29] M.G. Kim, Y. Shon, J. Lee, Y. Byun, B.S. Choi, Y.B. Kim, Y.K. Oh, Double stranded aptamer-anchored reduced graphene oxide as target-specific nano detector, Biomaterials 35 (2014) 2999–3004.
- [30] D. Wen, Q. Liu, Y. Cui, J. Kong, H. Yang, Q. Liu, DNA based click polymerization for ultrasensitive IFN-γ fluorescent detection, Sens. Actuators B Chem. 276 (2018) 279–287.
- [31] N. Tuleuova, C.N. Jones, J. Yan, E. Ramanculov, Y. Yokobayashi, A. Revzin, Development of an aptamer beacon for detection of interferon-gamma, Anal. Chem. 82 (2010) 1851–1857.
- [32] C.C. Chang, S. Lin, C.H. Lee, T.L. Chuang, P.R. Hsueh, H.C. Lai, C.W. Lin, Amplified surface plasmon resonance immunosensor for interferon-gamma based on a streptavidin-incorporated aptamer, Biosens. Bioelectron. 37 (2012) 68–74.
- [33] H.J. Kim, C.-H. Jang, Liquid crystal-based aptasensor for the detection of interferon-γ and its application in the diagnosis of tuberculosis using human blood, Sens. Actuators B Chem. 282 (2019) 574–579.
- [34] R. Gao, D. Lu, D. Guo, X. Xin, Dual-optofluidic waveguide in-line fiber biosensor for real-time label-free detection of interferon-gamma with temperature compensation, Opt. Express 28 (2020) 10491–10504.
- [35] G. Liu, C. Cao, S. Ni, S. Feng, H. Wei, On-chip structure-switching aptamer-modified magnetic nanobeads for the continuous monitoring of interferon-gamma ex vivo, Microsyst. Nanoeng. 5 (2019) 1–11.
- [36] J. Xia, D. Song, Z. Wang, F. Zhang, M. Yang, R. Gui, L. Xia, S. Bi, Y. Xia, Y. Li, L. Xia, Single electrode biosensor for simultaneous determination of interferon gamma and lysozyme, Biosens. Bioelectron. 68 (2015) 55–61.
- [37] Y. Liu, N. Tuleouva, E. Ramanculov, A. Revzin, Aptamer-based electrochemical biosensor for interferon gamma detection, Anal. Chem. 82 (2010) 8131–8136.
- [38] H. Jin, R. Gui, X. Gao, Y. Sun, An amplified label-free electrochemical aptasensor of γ-interferon based on target-induced DNA strand transform of hairpin-to-linear conformation enabling simultaneous capture of redox probe and target, Biosens. Bioelectron. 145 (2019), 111732.
- [39] H. Zhang, B. Jiang, Y. Xiang, Y. Chai, R. Yuan, Label-free and amplified electrochemical detection of cytokine based on hairpin aptamer and catalytic DNAzyme, Analyst 137 (2012) 1020–1023.
- [41] Y. Chen, T.S. Pui, P. Kongsuphol, K.C. Tang, S.K. Arya, Aptamer-based array electrodes for quantitative interferon-γ detection, Biosens. Bioelectron. 53 (2014) 257–262.
- [42] G. Xu, J. Abbott, L. Qin, K.Y. Yeung, Y. Song, H. Yoon, J. Kong, D. Ham, Electrophoretic and field-effect graphene for all-electrical DNA array technology, Nat. Comm. 5 (2014) 1–9.
- [43] G. Xu, J. Abbott, D. Ham, Optimization of CMOS-ISFET-based biomolecular sensing: analysis and demonstration in DNA detection, IEEE Trans. Electron Devices 63 (2016) 3249–3256.
- [44] J. DeChancie, K.N. Houk, The origins of femtomolar protein—ligand binding: hydrogen-bond cooperativity and desolvation energetics in the biotin—(strept) avidin binding site, J. Am. Chem. Soc. 129 (2007) 5419–5429.
- [45] D. Mao, J. Morley, Z. Zhang, M. Donnelly, G. Xu, High-yield passive Si photodiode array towards optical neural recording, IEEE Electron Device Lett 39 (2018) 524-527
- [46] Z. Xiong, F.J. Hwang, F. Sun, Y. Xie, D. Mao, G.L. Li, G. Xu, Spectrally filtered passive Si photodiode array for on-chip fluorescence imaging of intracellular calcium dynamics, Sci. Rep. 9 (2019) 1–9.
- [47] S.M. Sze, Y. Li, K.K. Ng, Physics of Semiconductor Devices, 2nd ed., 1998. Hoboken, NJ.
- [48] B.F. Matarèse, P.L. Feyen, A. Falco, F. Benfenati, P. Lugli, J.C. deMello, Use of SU8 as a stable and biocompatible adhesion layer for gold bioelectrodes, Sci. Rep. 8 (2018) 1–12.

- [49] D. Cai, L. Ren, H. Zhao, C. Xu, L. Zhang, Y. Yu, H. Wang, Y. Lan, M.F. Roberts, J. H. Chuang, M.J. Naughton, A molecular-imprint nanosensor for ultrasensitive detection of proteins, Nat. Nanotech. 5 (2010) 597–601.
- [50] P. Valdastri, E. Susilo, T. Förster, C. Strohhöfer, A. Menciassi, P. Dario, Wireless implantable electronic platform for chronic fluorescent-based biosensors, IEEE Trans. Biomed. Eng. 58 (2011) 1846–1854.
- [51] H. Zhang, G. Feng, Y. Guo, D. Zhou, Robust and specific ratiometric biosensing using a copper-free clicked quantum dot-DNA aptamer sensor, Nanoscale 5 (2013) 10307–10315.
- [52] J. Smestad, L.J. Maher III, Ion-dependent conformational switching by a DNA aptamer that induces remyelination in a mouse model of multiple sclerosis, Nucleic Acids Res. 41 (2013) 1329–1342.
- [53] A. Keefe, S. Pai, A. Ellington, Aptamers as therapeutics, Nat. Rev. Drug Discov. 9 (2010) 537–550.
- [54] K. Han, Z. Liang, N. Zhou, Design strategies for aptamer-based biosensors, Sensors 10 (2010) 4541–4557.
- [55] K.M. Song, S. Lee, C. Ban, Aptamers and their biological applications, Sensors 12 (2012) 612–631.
- [56] B. Dubertret, M. Calame, A.J. Libchaber, Single-mismatch detection using gold-quenched fluorescent oligonucleotides, Nat. Biotech. 19 (2001) 365–370.
- [57] D. Zhu, X. Zhou, D. Xing, A new kind of aptamer-based immunomagnetic electrochemiluminescence assay for quantitative detection of protein, Biosens. Bioelectron. 26 (2010) 285–288.

Zheshun Xiong received his B.E. degree in optoelectronics from University of Electronic Science and Technology of China in 2016. He is currently pursuing the Ph.D. degree in electrical engineering at University of Massachusetts Amherst, MA, USA. His current research interests include optoelectronic cell interfaces and biosensors.

Kewei Ren received his Ph.D. degree in the department of Chemistry and Chemical Engineering from Nanjing University in 2015. He is now a postdoctoral research associate at the University of Massachusetts, Amherst. His research interests mainly focus on developing electrochemical biosensor, cell imaging, and therapy methods based on DNA/RNA nanotechnology.

Matthew Donnelly received his B.S. degree in electrical and computer engineering from University of Massachusetts, Amherst, MA, USA in 2018. He is now pursuing the Ph.D. degree in electrical engineering at University of Massachusetts, Amherst., MA, USA. His current research focuses on bioelectronic devices for cell interfacing and health monitoring applications.

Mingxu You is an assistant professor of chemistry at UMass Amherst. He received his Ph. D. in Chemistry from the University of Florida in 2012. During his doctoral study, he focused on developing DNA aptamer-based devices for cancer diagnosis, targeted drug delivery, and cell membrane biophysical studies. Prior to joining UMass in 2016, he pursued his postdoctoral research at Weill Cornell Medicine, interested in developing RNA-based fluorescent sensors for imaging metabolites and signaling molecules in live cells. Dr. You has authored 70 journal articles and 3 book chapters. His research goal is to develop next-generation platforms to study cell biology and disease, based on the building block of life – nucleic acids.

Guangyu Xu received his B.S. and M.S. degrees from Tsinghua University. In 2011 he received his Ph.D. in Electrical Engineering from UCLA, where he studied the variability effects in graphene electronics. Afterwards, Dr. Xu received his postdoctoral training at Harvard University and MIT Media Lab, where he worked on all-electrical DNA arrays and multiplexed neuroimaging assays, respectively. He then joined ECE Department at UMass Amherst in 2016 as an Dev and Linda Gupta Endowed Assistant Professor. His current research interests include biosensing, neuroengineering, nanobiotechnology, and bioinformatics, aiming to offer new tools and methods for important biomedical applications.